

Cooling rate-dependent polymorphism in thermoplastic polyurethanes: effect of hard segments content

Zakarya Baouch^a, Katalee Jariyavidyanont^b, Lisa Moni^a, Leire Sangroniz^c, Elmar Pösel^d,
Alejandro Müller^{c,e,*}, René Androsch^{b,**}, Dario Cavallo^{a,***}

^a Department of Chemistry and Industrial Chemistry, University of Genoa, Via Dodecaneso 31, 16146, Genoa, Italy

^b Interdisciplinary Center for Transfer-Oriented Research in Natural Sciences (IWE TFN), Martin Luther University Halle-Wittenberg, 06099, Halle/Saale, Germany

^c POLYMAT and Department of Polymers and Advanced Materials: Physics, Chemistry and Technology, Faculty of Chemistry, University of the Basque Country UPV/EHU, Paseo Manuel de Lardizábal, 3, Donostia-San Sebastián, 20018, Spain

^d BASF, Polyurethanes GmbH, Elastogranstrasse 60, Lemförde, Germany

^e IKERBASQUE, Basque Foundation for Science, Plaza Euskadi 5, Bilbao, 48009, Spain

ABSTRACT

Thermoplastic polyurethanes (TPUs) are multi-block copolymers consisting of hard (HS) and soft segments (SS). The hard segment, based on 4,4'-methylenediphenyl diisocyanate and 1,4-butanediol (MDI/BD), crystallizes into two forms (Form I and Form II) depending on cooling conditions. While these polymorphs exhibit distinct mechanical properties, a detailed understanding of their formation conditions is lacking. This study explores how HS content and the cooling rate of the melt influence TPU polymorphism. Using conventional and fast scanning calorimetry, along with in-situ and ex-situ structural characterization, we developed a “polymorph map” correlating cooling conditions and HS content with final structures. For HS content above 50 wt%, both polymorphs coexist at cooling rates of 10–30 K/min, with Form I dominating as the cooling rate increases. Fully amorphous TPUs form at cooling rates >100–1000 K/min. At HS lower than 50 wt%, only Form I crystallizes. Pure Form II cannot form under non-isothermal conditions due to thermal degradation at rates below 1–3 K/min. Polarized light microscopy distinguishes the polymorphs: Form II displays birefringent spherulites. Quenched samples reveal a glass transition temperature linearly dependent on HS content, suggesting partial miscibility between HS and SS. These findings provide a framework for designing TPUs with tailored crystalline structures through precise control of HS content and processing conditions.

1. Introduction

Thermoplastic polyurethanes (TPUs) are linear multi-block copolymers comprising hard and soft blocks, typically referred to as hard and soft segments (HS/SS) in the literature. The hard blocks are formed by the reaction of a diisocyanate and a chain-extending diol or diamines, thereby constituting urethane-rich domains. In contrast, the soft blocks comprise low-medium molecular weight macrodiols, typically polyethers or polyesters [1,2], which can be extended by diisocyanates. Given the at least partial immiscibility between the two blocks [3–7], TPUs are micro-phase separated at room temperature. Furthermore, since the HS possess high glass transition and/or melting temperatures, whereas the SSs are liquid or rubbery at room temperature, a wide variety of mechanical properties of the final material can be obtained

simply by tuning the HS/SS ratio [1]. As such, TPUs can display a wide range of mechanical behaviors, from elastomeric to plastic. Indeed, at low HS content, the hard segments form physical crosslinks and reinforcement for the SS matrix at room temperature, whereas, at high HS concentration, the SS domains toughen the rigid HS matrix. The versatility of mechanical properties, to which also a variety of possible soft blocks, bond chemistries (e.g., urea, amid, etc ...), and possible chemical crosslinks contribute, allows the use of TPUs in a wide variety of advanced applications, including smart materials with shape memory properties [8,9].

Some of the most widely employed TPUs are those in which the hard segments consist of 4,4'-methylenediphenyl diisocyanate/1,4-butanediol (MDI/BD), while the soft segment often is poly (tetramethylene oxide) (PTMO). Focusing on this system, it is well known that

This article is part of a special issue entitled: Honoring C. De Rosa published in Polymer.

* Corresponding author. Polymat and Department of Polymers and Advanced Materials: Physics, Chemistry and Technology, Faculty of Chemistry, University of the Basque Country UPV/EHU, Paseo Manuel de Lardizábal, 3, Donostia-San Sebastián, 20018, Spain.

** Corresponding author.

*** Corresponding author.

E-mail address: dario.cavallo@unige.it (D. Cavallo).

<https://doi.org/10.1016/j.polymer.2025.128477>

Received 18 February 2025; Received in revised form 3 April 2025; Accepted 30 April 2025

Available online 30 April 2025

0032-3861/© 2025 The Authors. Published by Elsevier Ltd. This is an open access article under the CC BY license (<http://creativecommons.org/licenses/by/4.0/>).

the hard segments can crystallize upon cooling the melt or casting a solution of the polymer, forming different crystal polymorphs as a function of the crystallization conditions [10–13]. In detail, X-ray and electron diffraction experiments of oriented films of various MDI/BD-based TPUs and model compounds [12,13] revealed two different crystalline structures for the hard segments. The structures are characterized by a more contracted or extended conformation of the butanediol section of the HS repeating unit, named Form II and Form I, respectively. The more extended BD chain conformation favors inter-chain hydrogen bonding perpendicular to the chain axis. Form II exhibits 3-dimensional periodicity with the chains arranged in a triclinic lattice, while Form I is considered disordered and paracrystalline only. The structural disorder and conformational differences between the two polymorphs have recently been assessed by synchrotron pair distribution function analysis and infrared spectroscopy [14,15]. These analyses revealed the following information: i) in Form I, hydrogen bonding between nitrogen and the carbonyl oxygen occurs only in the [100] direction, and the diphenylmethane units adopt an “edge-to-face” packing; ii) in Form II, the stacks of bent chains are similar to those of Form I but the different conformation of the BD portion results in a different hydrogen bonding network; iii) the conformational differences between Form II and Form I arise from the urethane group’s internal bond rotation concerning the phenyl ring and the opening bond angle of phenyl-CH₂-phenyl.

Due to the different structures, Form II and Form I also possess distinct properties. For instance, despite the melting of TPUs being a very complex process involving significant melting-recrystallization phenomena of the HS [16–21], the more ordered Form II exhibits a melting temperature that is 15–30 K higher than that of the paracrystalline Form I [12,15,21,22]. It is proposed that, upon heating Form I, this polymorph melts at relatively low temperatures, and the resulting undercooled melt recrystallizes into Form II [21]. Regarding the supramolecular morphology, Form II exhibits birefringent spherulites [6, 10,18], [20], while the crystalline aggregates of Form I do not possess a birefringent pattern at the micrometer length scale [11,15,23]. The characteristic packing of the two polymorphs also leads to diverse mechanical properties, with the theoretical elastic modulus of Form II being much higher than that of Form I (almost 6.75 GPa vs. 1.31 GPa) [15]. In addition, the elastomeric properties, such as the permanent set and the hysteresis, are negatively affected by the presence of Form II [24]. Obviously, controlling polymorphism can lead to tailored properties in the final product, such as recently demonstrated in foamed TPUs [25].

Given the relevance of TPU’s hard segments’ polymorphic crystallization, the relation between melt crystallization conditions and structural outcome should be outlined. In general, it is known that Form II is formed at low undercooling or low cooling rates from the melt. Instead, Form I develops at higher cooling rates and lower crystallization temperatures. However, the exact crystallization conditions leading to one or the other polymorph are seldom reported [15,21,23]. For instance, for an MDI/BD-based TPU with approximately 75 wt% HS, the pure Form II crystallized from the melt at cooling rates lower than about 4 K/min at temperatures higher than 150 °C, while the formation of pure Form I requires cooling rates faster than 16 K/min [15]. The limiting temperature for the growth of pure Form II shifts to 130–135 °C for polymers of undefined composition [21,23], suggesting a role of HS content in the polymorphic crystallization. While some systematic studies exist on the effect of hard/soft segment ratio on the general crystallization and melting features of TPUs [26–29], the issue of polymorphism has been neglected so far.

Despite the extensive literature on the crystallization of HS in MDI/BD-based TPUs, some fundamental gaps in knowledge remain. In particular, two crucial aspects that merit a thorough investigation are: (a) the effect of HS content and (b) the effect of cooling rate and thermal history, especially when the employed parameters mimic processing conditions, on polymorphism. Therefore, these two issues are addressed in the present work by employing conventional and fast scanning

calorimetry in a wide range of cooling rates, coupled with structural characterization, on a set of model TPUs with varying hard segment content.

2. Experimental

2.1. Materials

The TPUs of the present work were produced by BASF Polyurethanes GmbH (Lemförde, Germany) using a one-shot process. The raw materials were sourced from BASF. These TPUs consist of 4,4'-methylendiphenyl diisocyanate (MDI) and 1,4-butanediol (BD), which form the hard segments (HS) of the urethane. The soft segments are composed of poly (tetramethylene oxide) macrodiol with a number-average molecular weight (M_n) of about 1000 g/mol and a polydispersity index of around 2. The TPU casts were ground into chips and then injection molded to create uniform sheets for testing. Before any measurement, these sheets were annealed at 100 °C for 20 h, a common procedure to enhance the phase separation between HS and SS. Table 1 presents the composition and further relevant properties of the TPU samples analyzed in this study.

3. Instrumentation

3.1. Differential scanning calorimetry (DSC)

DSC studies were conducted using a DSC250 (TA Instruments, Newcastle, Delaware, USA) under a nitrogen flow of 50 mL/min. The measurement signals temperature and heat-flow rate were calibrated with a high-purity indium standard. A fresh sample, weighing approximately 7 mg, was prepared for each measurement to prevent any thermal degradation influencing the results.

The DSC thermal protocol is described schematically in Fig. S1a of the Supporting Information. This protocol includes five steps and is designed to analyze the effect of cooling rate on crystallization and determine the subsequent melting behavior. First, the samples were heated from the loading temperature (40 °C) to a maximum temperature above the corresponding TPU melting temperature at 20 K/min. This maximum temperature was adjusted for each TPU according to the relative melting temperature (250 °C for TPU29 to TPU60, 260 °C for TPU70, and 270 °C for TPU80). The selected maximum temperature of the melt was then kept for 1 min to erase the thermal history, followed by a cooling step to 20 °C at varying rates (from 3 K/min to 30 K/min) to study the crystallization behavior. After being held at 20 °C for 1 min, the sample was finally reheated to above the melting temperature at a rate of 20 K/min to observe the melting behavior.

Thermal stability is a key factor in studying MDI/BD urethanes and thermoplastic polyurethanes (TPUs). Yang et al. [30] reported that significant degradation of MDI/BD urethanes occurs at approximately 200 °C when exposed for more than 5 min. Degradation can also occur in the solid state if the annealing time is sufficiently long, e.g., 2 h at 170 °C. Camberlin et al. [31] highlighted that the limited thermal stability of these urethane compounds complicates the study of their thermal transitions, as the MDI/BD hard segments, with a melting point

Table 1
Composition and properties of the studied TPUs.

TPU code	HS content [%]	MDI-BD average length	M_w [g/mol]	M_n [g/mol]	Polydispersity index (PI)
TPU29	29.6	2.2	99,000	45,000	2.2
TPU33	33.2	2.3	101,000	45,000	2.2
TPU50	50.0	3.7	98,000	43,000	2.3
TPU60	60.0	5.0	97,000	43,000	2.3
TPU70	70.0	7.6	93,000	41,000	2.3
TPU80	80.0	10.8	83,000	37,000	2.2

above 180 °C, degrade after melting. Hwang et al. [32] observed that degradation becomes detectable through infrared analysis in samples held above 180 °C for more than 5 min. The degradation involves, for instance, simultaneous depolymerization and repolymerization, leading to a different molecular weight distribution [30].

To mitigate these effects and ensure the reliability of our experimental results, fresh samples were used for each measurement, and exposure to high temperatures during isothermal conditions was limited to 1 min. We are aware that some degradation might still occur in our experiments. Still, the impact of molecular rearrangements on the results is minimized thanks to the optimized thermal protocols and the use of single samples each run.

3.2. Fast scanning chip calorimetry (FSC)

FSC was employed to determine cooling rates above which HS crystallization is suppressed and to estimate HS glass transition temperatures of the samples listed in Table 1. We used a Flash DSC 1 (Mettler-Toledo, Greifensee, Switzerland) connected to a TC100 intra-cooler (Huber, Offenbach, Germany). The sample support temperature was set to -90 °C, and the sample environment was purged with nitrogen gas at a flow rate of 35 mL/min. Samples with a thickness of about 10 µm were manually cut from the injection-molded test parts and reduced in their lateral dimension to 50–100 µm with the help of a scalpel and a stereomicroscope. Such specimens were placed on conditioned and temperature-corrected UFS 1 sensors, using silicon oil and a thin layer of gold leaf to enhance heat transfer and minimize mechanical distortion of the sensor membrane related to the thermal expansion of the polymer during measurement. Samples were heated at 60,000 K/min (1000 K/s) to the respective maximum temperature (see DSC section) and cooled after an equilibration time of 0.5 s–200 °C at the same rate. The TPUs were then cooled from 200 to 0 °C, at rates between 6 K/min (0.1 K/s) and 6000 K/min (100 K/s), to evaluate the critical cooling rate above which crystallization is suppressed, with the latter analyzed by the enthalpy of melting during subsequent fast heating. Note that we only started slow-cooling experiments at 200 °C to reduce possible degradation/cross-linking. Glass transition temperatures of non-crystallized hard segments were estimated during cooling and subsequent heating at 60,000 K/min (1000 K/s). Details of the FSC temperature-time profiles are available in the Supporting Information (Fig. S1b and c). All measurements were performed at least twice to ensure reproducibility.

3.3. Polarized-light optical microscopy (PLOM)

The effect of cooling rate on semicrystalline microstructures of TPU containing different hard-segment contents was investigated by hotstage microscopy, employing a THMS 600 hotstage (Linkam, Tadworth, UK) and a polarized-light DMRX microscope (Leica, Wetzlar, Germany) operated in transmission mode. The temperature-time protocol is shown in Fig. S1d of the Supporting Information file. First, a small piece of the sample was placed between glass coverslips, heated at 20 K/min to a maximum temperature well above the typically observed melting temperature of the sample, and equilibrated at that temperature for 3 min. We applied a maximum temperature of either 270 or 250 °C to TPU containing hard-segment contents higher or lower than 60 %, respectively. Then, the equilibrium melt was rapidly cooled at 50 K/min to lower temperatures of around 180–200 °C to avoid thermal degradation before being cooled at either 20 or 1 K/min to room temperature, which is below the HS glass transition temperature of the samples. Images of the structures were captured at room temperature using a Motic 2300 CCD camera mounted to the microscope. Reproducibility was checked by analysis of two individual specimens.

3.4. Wide-angle X-ray diffraction (WAXD)

WAXD measurements were performed using a MiniFlex diffractometer (Rigaku, Tokyo, Japan) equipped with a Cu K α X-ray source ($\lambda = 0.154$ nm). The measurements were conducted in a $\theta/2\theta$ scanning mode. One-dimensional (1D) scattering curves were obtained using SmartLab Studio software. The scanning parameters were set as follows: start angle of 5° and end angle of 40°, step size of 0.05° and scanning speed of 2.5°/min. The X-ray generator was operated at a voltage of 40 kV and a current of 15 mA. Sample preparation was carried out in the DSC by cooling the samples from the appropriate maximum temperature to room temperature at different rates (equal to those employed in Fig. S1a). A sample weight of approximately 12 mg was used, and the samples were manually removed from the aluminum pans before the WAXD measurements.

Temperature-resolved WAXD measurements were performed in transmission geometry using synchrotron radiation at the beamline BM26 of the European Synchrotron Radiation Facility (ESRF), Grenoble, France [33]. TPU70 was selected as a representative sample due to its high HS content and fast crystallization kinetics. A sample piece was cut and sealed in a DSC aluminum pan, then inserted in a DSC600 hot-stage (Linkam, Tadworth, UK) to apply a specific thermal history. X-ray scans were collected with an exposure time of approximately 12 s during cooling the sample from the melt at selected rates. The magnitude of the scattering vector q defined by $q = (4\pi/\lambda) \sin \theta$, where $\lambda = 0.10332$ nm is the wavelength of the X-ray source and 2θ the scattering angle, was calibrated using α -Al₂O₃. The sample-to-detector distance was 0.279 m. Patterns were recorded with a Pilatus 300K-W detector, and the azimuthal averaging of the 2D patterns were performed using the home-built routines of the BUBBLE software package to obtain the intensity as a function of q .

3.5. Nuclear magnetic resonance spectroscopy (NMR)

The ¹³C NMR spectra were acquired on a JEOL 400 spectrometer operating at 101 MHz and maintained at a temperature of 50 °C \pm 1. Samples (20–25 mg) were dissolved in 1 mL of N,N-dimethylformamide-d₇ (DMF-d₇), with chemical shifts reported in ppm using the residual solvent signal at 34.89 ppm as an internal reference. The measurements were performed with 3.7 µs (30°) pulse width, 1.3 s acquisition time, a relaxation delay of 2.5 s, and 5000 scans at a temperature of 50 °C. Data processing was conducted using MestReNova (Mestrelab Research, v. 15.1), including manual phase correction, 64 k zero-filling, a 5th-order polynomial baseline correction, and apodization with a line-broadening factor (LB) of 0.5 Hz. Lorentzian deconvolution was applied for signal integration.

The signal of the tertiary aromatic carbon resonance was analyzed to extract information on the various dyads of MDI-BD and MDI-PTMO. Chemical shifts were calculated based on the assignment described in Ref. [34]. From the integration of the peaks indicated in Fig. S2 of the Supporting Information, the average length of MDI-BD units was determined following the analysis approach outlined in Ref. [35].

3.6. Gel permeation chromatography (GPC)

The molar mass of the samples and its distribution were determined using a GPC system equipped with two columns connected in series: PSS-Gel (100 Å, 5 µm, 300*8 mm) and Jordi-Gel DVB (Mixed-Bed, 5 µm, 250*10 mm). The column temperature was maintained at 60 °C, with a flow rate of 1 mL/min, and detection was carried out using a refractive index (RI) detector. Hexafluoroisopropanol was used as the mobile phase. The GPC measurements were performed in accordance with DIN 55672-2 (2008). The system was calibrated using polymethyl methacrylate (PMMA) standards (EasyCal; PSS, Mainz).

4. Results and discussion

4.1. Calorimetric analysis of crystallization

Fig. 1 presents DSC scans obtained during cooling from the melt (a) and subsequent heating (b) of TPUs of various HS content, recorded at a rate of 20 K/min. The data of Fig. 1a reveal non-isothermal crystallization with kinetics that depend on the HS content, with the data suggesting a non-monotonic trend. A major crystallization peak can be observed for all the TPUs. For TPU29 and TPU33, the crystallization peak temperatures are approximately 84 and 92 °C, respectively. As the HS content increases (TPU50, TPU60, and TPU70), the crystallization peak shifts to higher temperatures, from 112 °C for the polymer with an HS content of 50 wt% to 117 °C in the TPU with 80 wt% hard segment content. This indicates an acceleration of the non-isothermal crystallization kinetics as the hard segments become more concentrated, possibly also due to an increase in the average HS length [35].

Notably, TPU60 and TPU70 exhibit additional small exothermic shoulders at higher temperatures, around 135–140 °C, which are better appreciated in the close-up of Fig. S3a. These small peaks might indicate, as will be explained below, that the formation of the high-temperature modification Form II is not completely inhibited, and some traces of this polymorph are still forming under the applied cooling rate of 20 K/min. Interestingly, when the hard segment content is further increased to 80 wt%, the overall non-isothermal crystallization kinetics ceases to be accelerated and slows down instead. In fact, the crystallization peak temperature decreases a few degrees with respect to that of TPU70, but, more remarkably, the crystallization enthalpy is by far smaller than that of any other TPU cooled at an identical rate. The reason for this sudden decrease in the crystallization kinetics could be the proximity of the crystallization temperature to the hard segment-rich phase glass transition temperature, which, as judged by the cooling curve in Fig. 1a and on the basis of the literature [36], is around 75–80 °C for this particular HS/SS ratio. Therefore, HS crystallization, which occurs close to the glass transition temperature, might become diffusion-limited.

The melting curves of the TPUs, as shown in Fig. 1b, are rather complex after cooling the equilibrated melt at 20 K/min. In fact, the endothermic peaks are broad for all the samples and feature multiple events, which agrees with previous reports suggesting extensive melting, recrystallization, and re/melting of the HS crystalline domains on heating [16–20]. The multiple melting behavior could also be ascribed to the polydispersity in HS lengths. [37] melting For the interest of the present work, we note that TPU60 and TPU70, which

showed a small high-temperature shoulder at the main crystallization peak in the cooling curves (Fig. 1a and Fig. S2a), also display extra high temperature melting peaks, located between 220 and 230 °C (see close-up of Fig. S3b). Such melting endotherm might be the signature of a minor fraction of Form II HS crystals formed during cooling, which melt at temperatures higher than those of Form I [12,15,21,22]. However, as recently proposed [21], the possibility of Form I melting and recrystallizing into Form II cannot be excluded, mainly because the minor high-temperature melting peak is also present for TPU80, which does not show any high-temperature crystallization event upon cooling. Finally, the sluggish non-isothermal crystallization kinetics of TPU80 is also apparent from its heating curve, which exhibits a large heat capacity step at the glass transition at approximately 80 °C, followed by a major cold-crystallization event peaked around 110–120 °C.

The samples were cooled at rates between 3 and 30 K/min. The lowest rate was set just high enough to minimize thermal degradation. The capability of the instrument predefined the highest achievable rate. The recorded cooling curves (Fig. 2a and c) generally show two distinct exothermic events. According to the literature [15,21], the low-temperature peak is attributed to the paracrystalline Form I polymorph, whereas the high-temperature peak is associated with Form II (see arrows). As the cooling rate increases, the enthalpy of the high-temperature peak gradually decreases. It disappears above a critical cooling rate that depends on the hard-segment content and can be estimated by visual inspection (10 K/min for TPU50 and 15 K/min for TPU80). Fig. S4 shows that TPU60 and TPU70 exhibit similar behavior, whereas TPU29 and TPU33 show only the low-temperature Form I peak for all cooling rates. How the critical cooling rate to obtain a predominant Form I depends on the HS content is explained later in the text.

Regarding the melting behavior after a given cooling history (Fig. 2b and d), consistently with the presence of two crystallization peaks in the cooling curves, a high-temperature peak or portion of melting endotherm is also present (see arrow). Such peak or portion of a peak is located between 200 and 220 °C, for cooling rates ranging from 3 to 7.5 K/min for TPU50; and above 220 °C for TPU80. For TPU80 the peak is present for all the cooling rates, but its area decreases to a constant value going from 3 to 15 K/min. This aligns with Form II's known higher melting temperature compared to Form I. It supports the interpretation that the two crystallization events correspond to the simultaneous formation of high- and low-temperature polymorphs. Thus, the proportions of these polymorphs vary depending on the cooling rate. Also, the extremely slow crystallization of TPU80 is evident from its cooling rate-dependent melting behavior. Complete crystallization, indicated by the

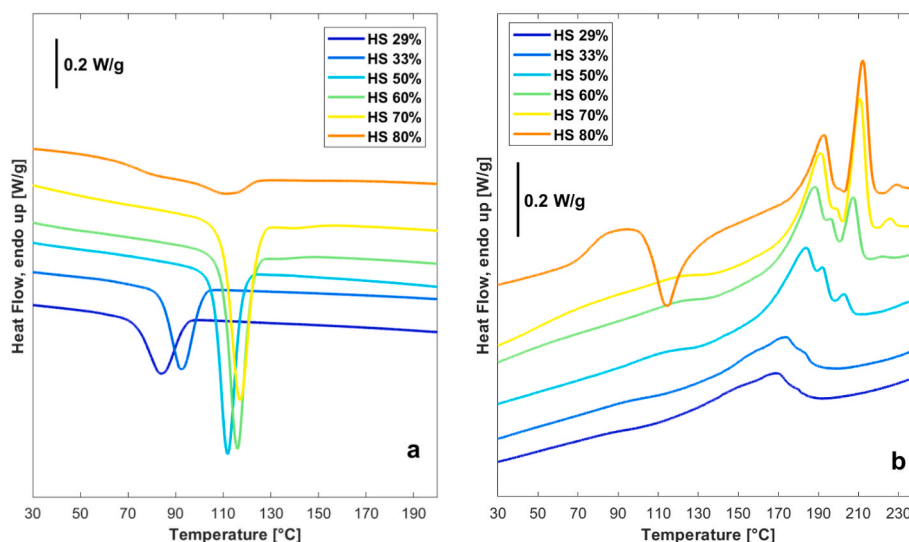


Fig. 1. DSC cooling (a) and heating (b) scans of different TPUs recorded at 20 K/min.

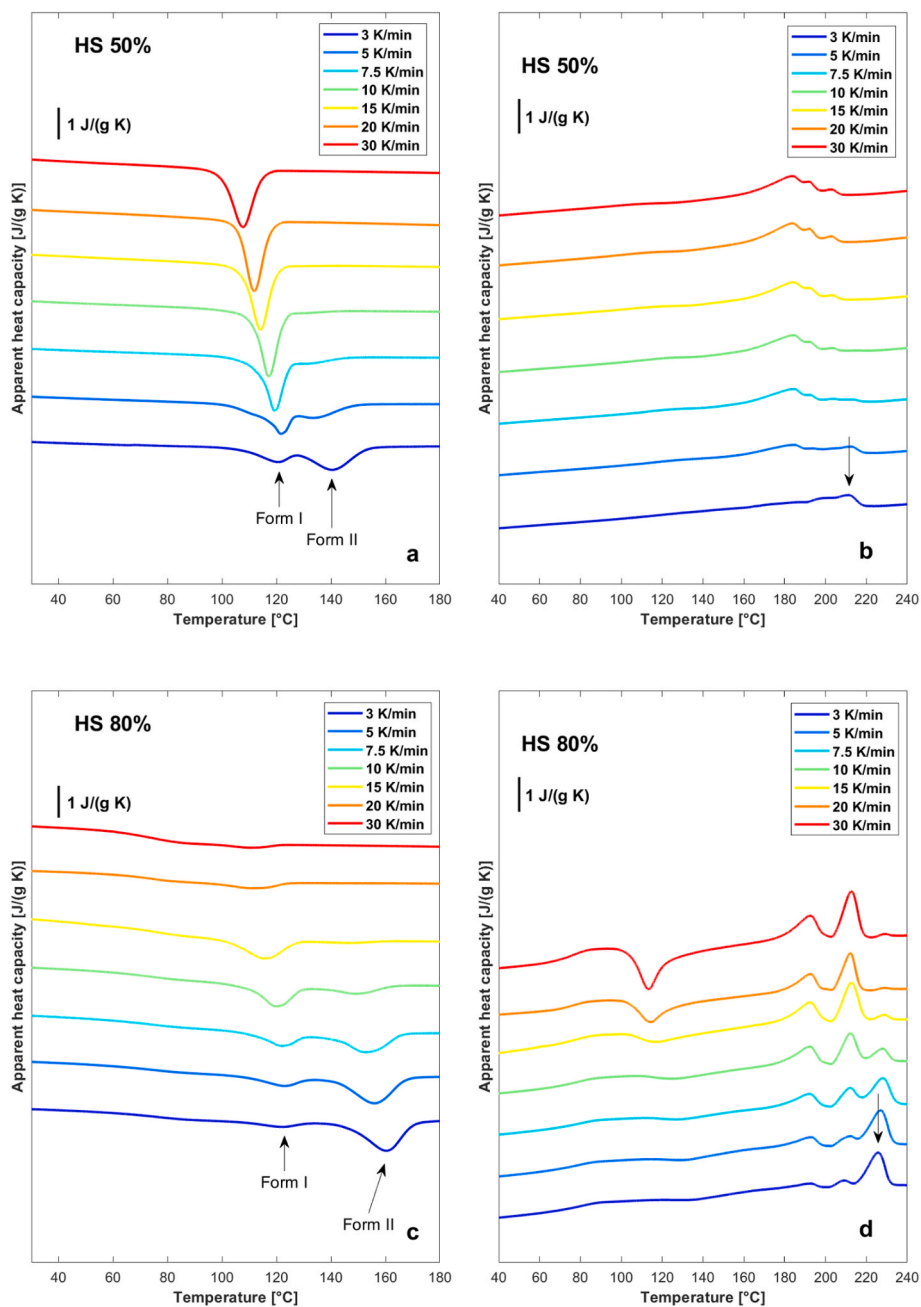


Fig. 2. DSC cooling (a, c) and subsequent heating (b, d) scans for TPU50 (a, b) and TPU80 (c, d) cooled at the indicated rates.

minimal cold-crystallization peak during subsequent heating, was only achieved at cooling rates of up to 10 K/min. Faster cooling resulted in a progressively higher fraction of amorphous hard segments (HS).

If different heating rates for a given cooling history would be applied, information on the reorganization behavior of the initial structure could be achieved. Since this is not the focus of the current work, we refer the interested reader to previous literature where the topic of multiple melting of TPUs has been addressed [16,20,21].

Fig. 3 summarizes the DSC measurement results for all samples. The crystallization temperature decreases with increasing cooling rate for both polymorphs and all materials (Fig. 3a). For Form II (higher crystallization temperature), the crystallization temperature increases with higher HS content, but no Form II crystallization is observed for materials with HS content below 50 %. For Form I, the trend is less clear: the crystallization temperature increases as HS content rises from 29 % to 50 %, then remains constant or varies in a narrow range. Notably, the

sample with 80 % HS crystallizes into Form I at slightly lower temperatures than samples with 60–70 % HS content.

Fig. 3b shows the enthalpy of Form II crystallization for various TPUs as a function of cooling rate. The plot provides insights into the disappearance of the high-temperature crystallization peak (Form II) with increasing cooling rate, depending on the hard segment (HS) content. It reveals the cooling rate at which only Form I develops under non-isothermal conditions. For TPU29 and TPU33, Form II does not appear even at the lowest cooling rates. A decrease in Form II enthalpy with an increasing cooling rate is always observed for the other materials. The critical cooling rate needed to suppress Form II crystallization increases from 50 wt% HS (15 K/min) to 70 wt% HS (30 K/min). However, for an 80 wt% HS content, the cooling rate required to suppress Form II decreases to 20 K/min.

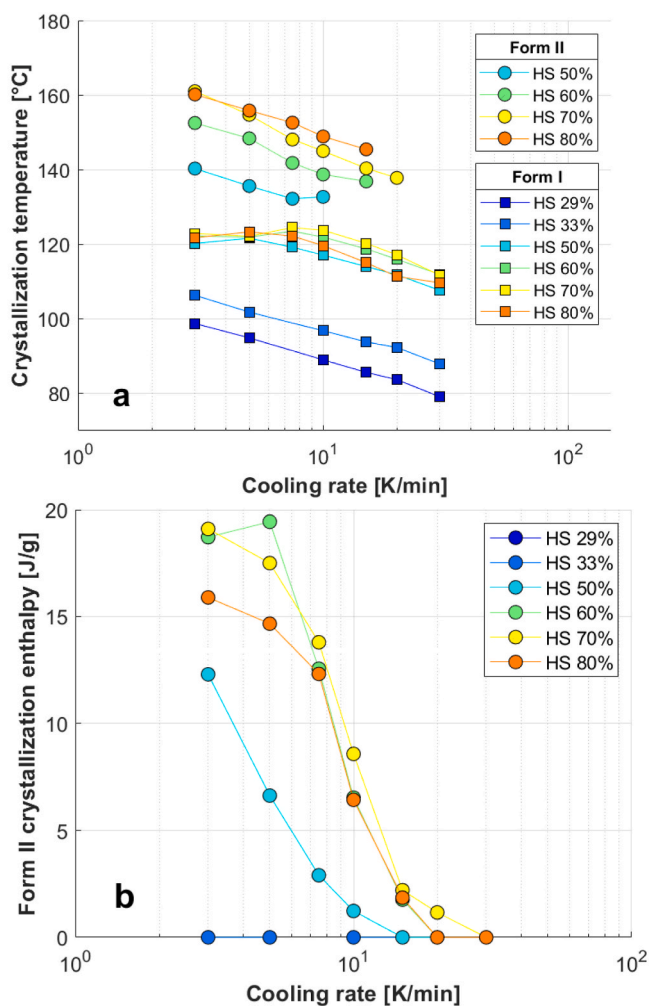


Fig. 3. Crystallization temperatures for the two polymorphs (a) and Form II crystallization enthalpy (b) as a function of the cooling rate for the various TPUs.

4.2. Polymorphic crystallization analysis by temperature-resolved synchrotron WAXD

In-situ synchrotron WAXD crystallization experiments were conducted on a selected sample to validate the formation of specific crystal polymorphs. The chosen TPU has a hard segment content of 70 wt%, which suggests a significant degree of crystallinity and reasonably fast crystallization kinetics. Fig. 4 presents the wide-angle X-ray diffractograms during cooling from the melt of TPU70 at two rates: 7.5 K/min in

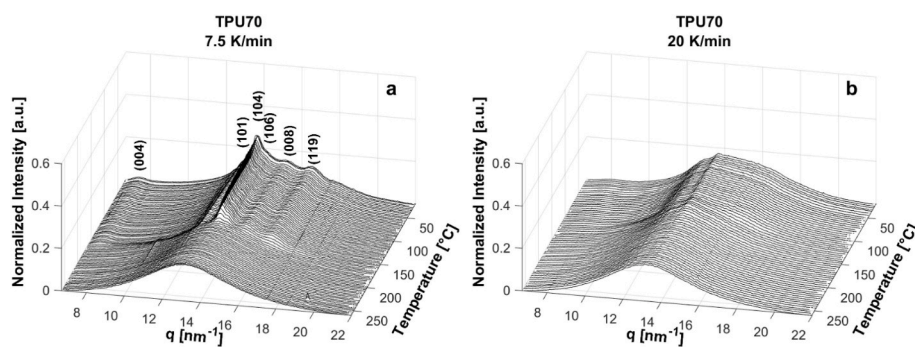


Fig. 4. Temperature-resolved synchrotron WAXD patterns during cooling the melt of TPU70 at 7.5 K/min (a) and 20 K/min (b). Diffraction peaks of Form II are indexed according to the literature [15,37].

panel a and 20 K/min in panel b. According to the DSC cooling curves (Fig. S4g), lower cooling rates form both Form II and Form I, while higher rates lead to the predominance of the paracrystalline Form I. Clear diffraction peaks are observed during cooling at 7.5 K/min, around 160–170 °C (Fig. 4a). These diffraction patterns are consistent with those characteristic of the more ordered Form II. [11–13,15,21]. However, the simultaneous formation of Form I during continued cooling, as predicted by the DSC curve around 140 °C, is not detected due to its low quantity and paracrystalline nature. Conversely, at a higher cooling rate of 20 K/min (Fig. 4b), the crystallization of Form II is nearly suppressed. Consistent with the DSC curve in Fig. S4g showing a single exotherm attributed to the paracrystalline Form I, the amorphous halo is superimposed by peaks indicating Form I formation at around 130–120 °C, albeit at low intensity.

To gain further insights into the final structural outcomes of TPUs with varying HS content, WAXD patterns were also collected in-house at room temperature following cooling from the melt at different rates.

4.3. Room-temperature WAXD after different cooling rates

Fig. 5 shows, as an example, the variation of room temperature WAXD patterns with varying cooling rates for two representative samples with different hard segment content. At low cooling rates, only a few distinct diffraction peaks appear, superimposed on a broad, amorphous halo, with the most prominent peak centered around 19.5° (2θ). This pattern corresponds to the crystalline Form II, which is well-documented in the literature to form at low cooling rates and high crystallization temperatures [11–13,15,21]. It is important to note that crystallinity decreases with lower hard segment content, as observed for TPU50 compared to TPU80. As the cooling rate increases, for both samples, the crystalline peaks of Form II are replaced by a broad halo and a faint peak around 11.5° (2θ) (indicated by the arrow), signifying the transition to the more disordered Form I. These features become less distinct at the highest cooling rate for TPU80, aligning with the DSC cooling curve shown in Fig. 2, where the material approaches near-complete amorphization at 30 K/min. The WAXD patterns for both samples are consistent with the DSC cooling curves from Fig. 2, showing a slight difference in the critical cooling rate required for the transition from a dual crystalline structure (Form II + Form I) at lower rates to the predominance of Form I at higher cooling rates.

Similar observations can be made from the WAXD patterns obtained for the other TPU samples cooled at different rates, as shown in Fig. S5. Specifically, the formation of Form II in TPU29 and TPU33 cannot be confirmed, as diffraction peaks are absent even at the lowest cooling rate applied. This aligns with the presence of a single exothermic event in DSC cooling scans and previous literature results for samples with similar HS content [34]. In contrast, TPU60 and TPU70 exhibit a clear dependence of polymorphism on the cooling rate, with Form II appearing more persistent at higher cooling rates for TPU70.

It is worth noting that calculating the crystallinity of TPU from the

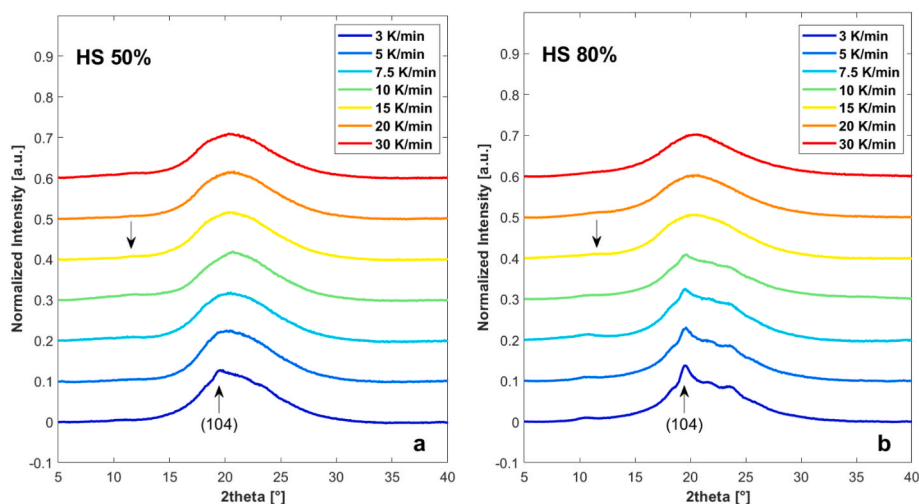


Fig. 5. WAXD patterns at room temperature for TPU50 (a) and TPU80 (b) cooled at the indicated rates. For clarity, only the most intense diffraction peak of Form II has been indexed.

WAXD patterns is not an easy task, particularly in this case, where two different structures form under most crystallization conditions. Therefore, we chose not to address this issue, as we believe it would not yield more meaningful information compared to what has been obtained through quantitative calorimetry and qualitative WAXD identification of the two structures.

4.4. Critical cooling rate to suppress ordering

After determining the critical cooling rates needed to suppress Form II crystallization in most TPUs using DSC and WAXD, the cooling conditions necessary to prevent any ordering and achieve a fully amorphous sample are outlined below. Fig. 6 presents a series of fast scanning calorimetry curves recorded during heating at 1000 K/s after cooling at 1000 K/s after cooling either TPU50 (Fig. 6a) or TPU80 (Fig. 6b) at the indicated rates.

Fast cooling at, e.g., 100 K/s (red curves) fully suppresses both Form

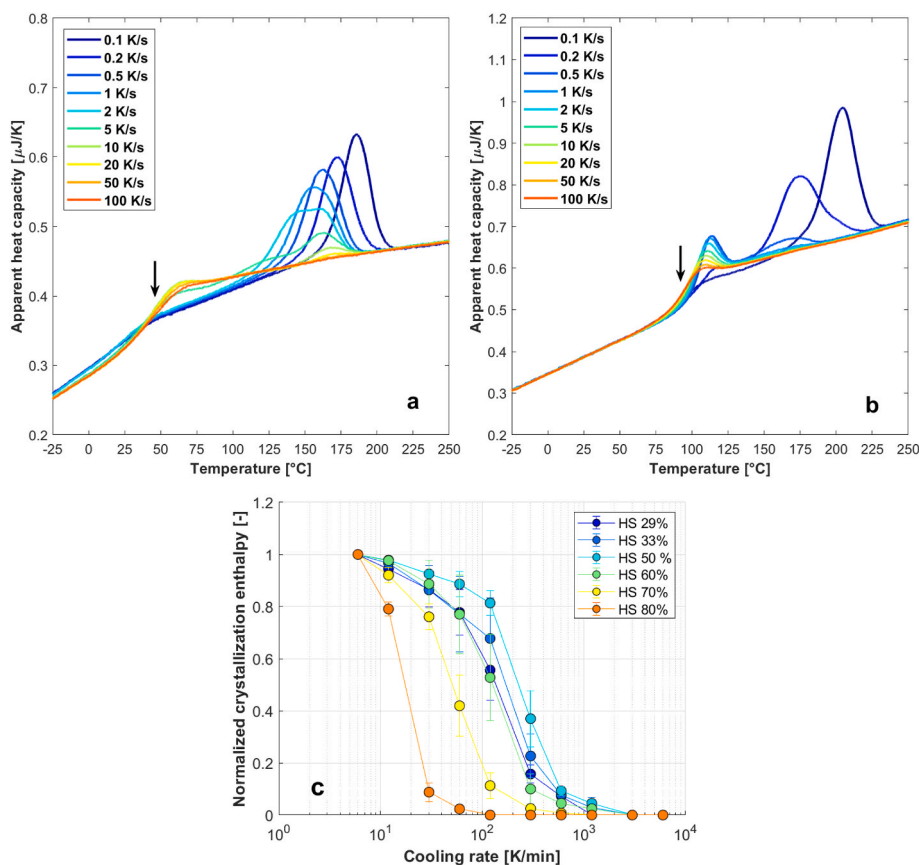


Fig. 6. Selected heating FSC scans at 1000 K/s after cooling at the indicated rates for TPU50 (a) and TPU80 (b). Normalized crystallization enthalpy as a function of the cooling rate for the various TPUs (c).

II crystallization and Form I paracrystalline phase formation, as is indicated by the absence of endothermic melting in the heating scans in both samples. Instead, only a glass transition of either phase-separated hard segments or a solution of hard and soft segments is detected (see arrows); note that the endothermic event superimposed to the glass transition in the case of TPU80 is an enthalpy-recovery peak caused by physical aging of the glassy amorphous phase [38], scaling in area with the time of (non-isothermal) annealing the glass during cooling and heating. With a decreasing cooling rate, the heat-capacity step at the glass transition temperature decreases, and melting peaks appear, indicating that the sample crystallized during the cooling step. However, conclusions cannot be drawn on whether these peaks are associated with the melting of Form II crystals or the disordering of Form I. The observed shift of the melting peaks to higher temperatures with decreasing cooling rates is likely caused by the increase in the crystallization temperature, as demonstrated in Fig. 2a and c. Plotting the enthalpy of melting as a function of the cooling rate then yields the critical cooling rate above which ordering is suppressed. For the shown examples of in TPU50 and TPU80, values of around 50 and 2–5 K/s, respectively, were obtained. These results are consistent with the DSC experiments discussed above, which also suggested faster crystallization in the case of TPU50.

The crystallization enthalpy of the various samples, normalized by the highest absolute value observed after slow cooling, is plotted versus the cooling rate in Fig. 6c to gain quantitative information on the critical cooling rate to suppress ordering. From the plot, it is deduced that the critical cooling rate for amorphization of the TPU is relatively constant in the HS content range from 29 to 60 wt%, being around 1000–2000 K/min. However, further increasing the HS content to 70 and 80 wt%, the cooling rate required to obtain a fully amorphous sample decreases to about 100 K/min. This result confirms the slower overall crystallization kinetics of samples with high HS content.

4.5. Glass transition temperature of amorphous TPU

With the capability to suppress crystallization by fast cooling, the glass transition temperatures of the various TPUs were analyzed, focusing on the relative change related to the hard segment content. For example, Fig. 7a shows with the blue curve the apparent heat capacity of TPU80 obtained during cooling the sample at 1000 K/s, while the red curve is its first derivative, used to estimate the glass transition temperature by the obtained maximum. Similar data were obtained for all TPUs, with their glass transition temperatures plotted as a function of the hard segment content in Fig. 7b. The data reveal a linear increase in the glass transition temperature with the hard segment content. This qualitatively agrees with a former glass-transition study performed on a different MDI-BD-based TPU system containing epoxidized hydroxyl-terminated polybutadiene as a soft segment [36]. Also, in that case, a

single glass transition temperature was obtained in quenched and, therefore, non-crystalline samples of different hard segment content, suggesting miscibility of amorphous hard and soft segments.

A similar observation for the same systems has been reported by Balko et al. via FSC measurements [20]. The occurrence of a single, HS content-dependent glass transition temperature in the case of quenched and non-crystalline samples led the authors to conclude that HS and SS were fully miscible in the amorphous state. Further experiments with stepwise isothermal crystallization suggested that the crystallization process of the hard segments drives phase separation in these TPUs [20].

It is interesting to extrapolate the present experimental glass transition temperature data to the extremes of the TPU compositions and compare them with the results reported in the literature for neat poly (BDI/MD) and neat PTMO (see Fig. 7b). The extrapolated value for the T_g of the neat HS is consistent with the reported value for a neat MDI/BD polymer [28,40]. The situation is more complex at the other extreme of the composition scale (0 wt% HS). Indeed, the measured T_g of a neat PTMO with the same molecular weight as that adopted to prepare the TPU of this work is around -83 °C, as measured with temperature-modulated DSC [39]. On the other hand, our extrapolated value is much higher, closer to -60 °C. Despite the obvious difference in scanning rate between our measurements (1000 K/s) and the literature one (3 K/min), we suggest that a tethering effect of the PTMO chain ends to the hard segments can cause the increase in the T_g value for the soft segment. In fact, the value extrapolated at 0 wt% from the data in the range of 29–80 wt% HS is in good agreement with the measured value of the SS of the same molecular weight as part of a TPU [39]. Nevertheless, partial miscibility between HS and SS in this case cannot be excluded.

4.6. Micrometer-scale semicrystalline morphology of non-isothermally crystallized samples

Fig. 8 shows PLOM micrographs of TPU29, TPU50, TPU70, and TPU80 (from left to right), with the structures obtained by cooling the melt at 20 (top row) and 1 K/min (bottom row). Regarding TPU50, TPU70, and TPU80, cooling the melt at 1 K/min allows space-filling spherulitic growth of Form II, with the spherulite diameter depending on the HS content, increasing from about 50 μm in the case of TPU50 to >100 μm in case of TP80. When the cooling rate is increased to 20 K/min, due to the increase in the nuclei density by lowering the crystallization temperature, many small Form II spherulites with a diameter of about 10 μm are observed; however, they do not yield a space-filled structure. Due to continuous cooling, Form II spherulite growth stops, and the small spherulites appear dispersed in a continuous non-birefringent and featureless — matrix, which, however, is composed of amorphous phase and Form I paracrystalline phase, with the latter suggestion based on additional experiments described below. For TPU29, regardless of cooling at 20 or 1 K/min, the formation of

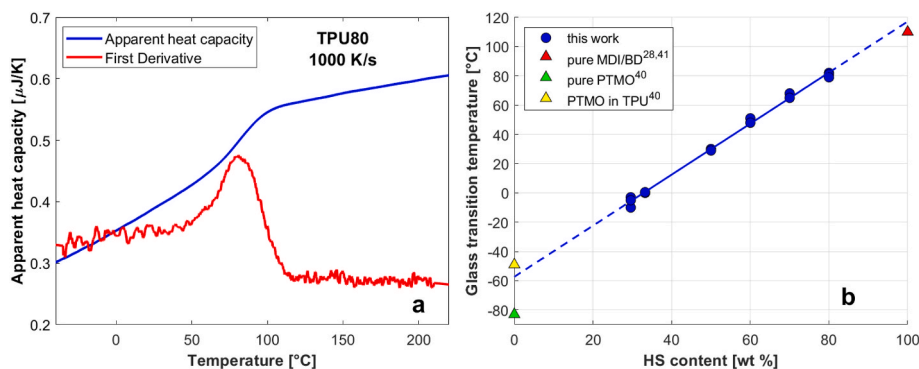


Fig. 7. a) FSC scan of amorphous TPU80 obtained during cooling at 1000 K/s (blue), and its first derivative (red); b) Glass transition temperature as a function of the HS content. The literature data are taken from Ref. [39] for the pure PTMO and PTMO in TPU and from Refs. [28,40] for the pure poly(MDI/BD). (For interpretation of the references to color in this figure legend, the reader is referred to the Web version of this article.)

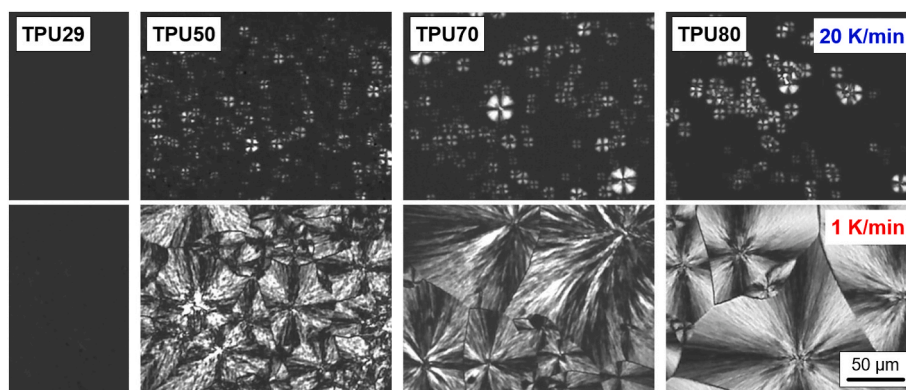


Fig. 8. PLOM micrographs of TPU29, TPU50, TPU70, and TPU80 (from left to right) crystallized by cooling from the melt at 20 (top row) and 1 K/min (bottom row). The scale bar of 50 μm holds for all images.

birefringent spherulites is not detected, suggesting the formation of Form I only, confirming calorimetric experiments.

In fact, in the case of slowly cooled TPU29, similar results as described in the literature were obtained [11,23], as rather large non-birefringent objects/spherulites were detected by varying the imaging conditions (insertion of a lambda plate, see Fig. 9a and b). These objects appear much smaller on fast cooling at 20 K/min and are also evident in samples of higher HS content.

The PLOM structure of TPUs containing the Form I is confirmed by cold-ordering (formation of the paracrystalline phase from the glassy state) a sample at around 100 °C in the DSC, thus containing a relatively large amount of Form I, and subsequent inspection of its structure by PLOM. Fig. 10a shows the temperature-time profile of the crystallization experiment applied to TPU80, including quenching the melt from 270 °C at a supercritical rate to room temperature, suppressing any ordering. The obtained amorphous sample was then heated to 120 °C to allow detectable cold-ordering, that is, the formation of the Form I paracrystalline phase, as sketched by the red-colored exothermic cold crystallization peak. The plot of Fig. 10b shows the DSC cold-ordering peak, thus proving the presence of ordered structures after re-cooling the sample to room temperature. The gray curve is a complete heating scan of the quenched sample, providing evidence of the absence of ordering during prior quenching as similar areas of exothermic cold-ordering and endothermic melting are obtained, with the dotted line approximating the liquid heat capacity. Fig. 10c, finally, shows the PLOM image of TPU80 containing a relatively large amount of Form I, confirming the interpretation of the PLOM images of Fig. 8. Note that the absence of ordered structure after quenching and Form I cold-ordering was additionally confirmed by WAXD (not shown).

4.7. Structural map of polymorphic TPU crystallization

From the collected calorimetric and structural data, we can build a “structural map” of the studied TPUs, with the variables cooling rate and HS content (Fig. 11). Such a diagram is constructed by reporting the critical cooling rate for obtaining a given polymorph, a combination of them, or the lack of any ordered structure as a function of the hard segment content of the different samples. The critical cooling rate above which the samples remain completely amorphous is derived from the vanishing crystallization enthalpy obtained via FSC (Fig. 6c). The region of the map suggesting the presence of Form I only is calculated from Fig. 3b by looking at the occurrence of a single low-temperature crystallization peak in the DSC and suppression of the high-temperature exothermic peak. Two crystallization events in the DSC are recorded below this critical cooling rate, i.e., inside the “Form II + Form I’” region.

It is important to notice that, as previously mentioned, cooling rates lower than approximately 1–3 K/min lead to thermal degradation of the polymer (especially those with high HS content). This phenomenon has been probed by means of crystallization kinetics, which is known to be very sensitive to polymer molecular features (molar mass, chemistry, etc.). In particular, it has been proven that the effect of thermal degradation on crystallization kinetics is detectable in an easy and highly sensitive way also for TPUs [41]. Therefore, in our case, thermal degradation was judged from the measured crystallization and melting enthalpy at low cooling rates, which decreased with respect to the one recorded at higher cooling rates. Consequently, we conclude that achieving “pure” Form II via non-isothermal crystallization at low rates in these samples is impossible due to concurrent thermal degradation. However, hypothetically, by cooling sufficiently slowly, the major portion of hard segments should crystallize completely in Form II, not leaving enough HS for the subsequent development of Form I at lower crystallization temperatures. For this reason, a hypothetical “Form II

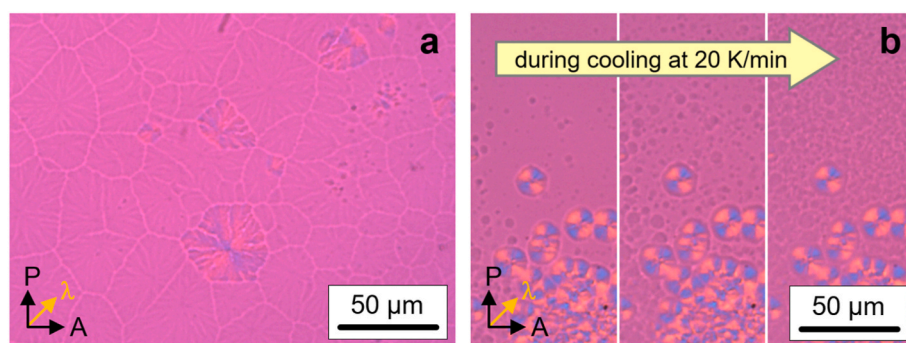


Fig. 9. PLOM micrograph of non-birefringent objects/spherulites of TPU29 taken at room temperature after cooling the melt at 1 K/min (a) and PLOM images of structural evolution of non-birefringent objects in TPU50 captured during cooling at 20 K/min (b).

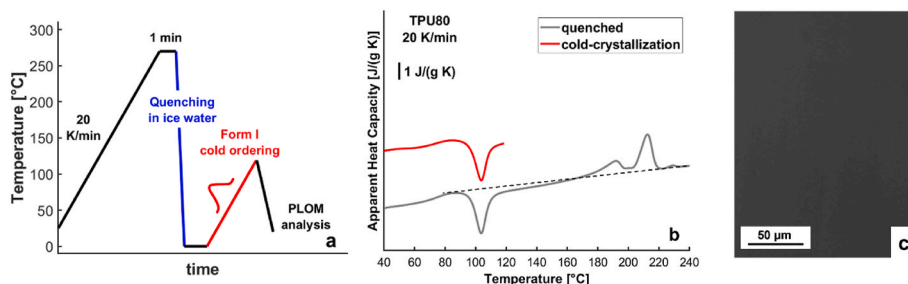


Fig. 10. DSC thermal profile employed for preparation of TPU80 containing only Form I besides amorphous structure (a), DSC thermal program with Form I cold-ordering indicated (b) at around 100 °C, and (c) the corresponding PLOM image after cooling the cold-ordered sample to room temperature(c). The gray curve in (b) is a complete DSC scan of initially amorphous TPU80, revealing the melting behavior after cold-ordering.

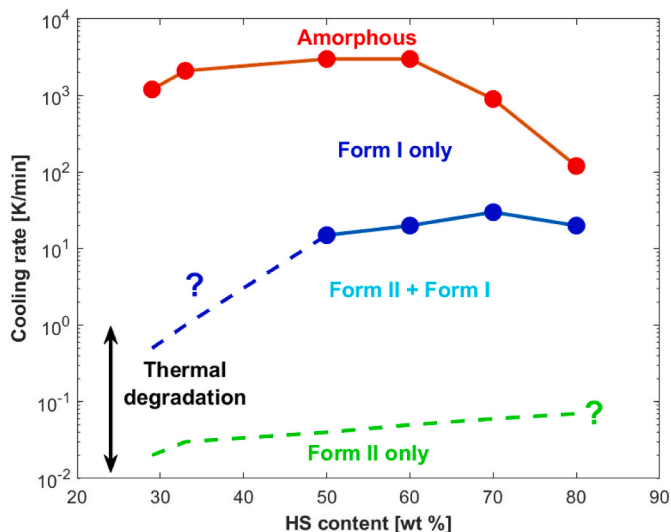


Fig. 11. Structural map of the various TPU as derived from DSC/FSC measurements: cooling rate required to obtain a given structural outcome (amorphous, Form I only, Form I + Form II, and Form II only) as a function of HS content. Blue data points are obtained with DSC, and red data points with FSC. The range of cooling rates in which thermal degradation occurs, determined as explained in the text, is also highlighted. (For interpretation of the references to color in this figure legend, the reader is referred to the Web version of this article.)

only” region is indicated with a dashed boundary in the diagram.

Moreover, we note that for the lowest HS content (TPU29 and TPU33), two peaks are not evident in the DSC cooling scans, even at the lowest applicable rates, and no apparent Form II diffraction peaks were detected by WAXD (Fig. S5) either. Hence, we assume that these samples always crystallize into Form I, and we are thus unable to define the boundary between the “Form I only” and “Form II + Form I” regions of the diagram for this HS content range. For this reason, a transition from the behavior of HS 29 % and the clearly detected boundary at HS contents above 50 % is again suggested with a dashed blue line. However, the existence of a critical amount of hard segments in the multiblock copolymer to produce the ordered Form II might be required. This hypothesis could be further tested with isothermal crystallization experiments at relatively high temperatures, which is out of the scope of the present work.

Finally, we note that the critical cooling rate to enter the “Form I only” region (blue data points) is relatively constant or increases only minimally with HS content between 50 and 70 %, then it decreases slightly for TPU80. This might indicate that the overall crystallization rate of Form II is not highly dependent on the hard segment content.

The critical cooling rate for amorphization (red data points) shows the largest variation among the samples due to the differences in the

overall crystallization rate of Form I. In addition, the trend with respect to HS content is non-monotonous. Notably, the critical amorphization rate decreases from above 3000 K/min to around 100 K/min when the HS content is increased from 60 to 80 wt%. This might result from the simultaneous increase in the polymer (or HS-rich phase) glass transition temperature (Fig. 7), which causes TPU80 crystallization, occurring close to the glass transition, to be limited by polymer chain diffusion.

On the basis of the reported data, it is possible to understand the mechanism driving polymorph selection as a competition between two different structures, each possessing its own melting temperature, which develop at different (temperature and HS-dependent) rates. According to the respective melting temperatures [12,15,21,22], Form II is the thermodynamically more stable structure, while Form I is a metastable structure. Considering a given TPU with HS content higher than 50 wt percent, the thermodynamically more stable structure (Form II) is also kinetically favored at lower undercooling (higher crystallization temperatures or lower cooling rates), where the metastable Form I can not develop at meaningful rates. Thus, Form II becomes the predominant crystallization product due to both thermodynamic and kinetic reasons at high crystallization temperatures. Conversely, with increasing cooling rates (decreasing crystallization temperatures), we also undercool Form I and its formation becomes faster than that of Form II in the considered temperature range. Therefore Form I becomes the predominant structure in fast (er) cooled samples. The situation is schematically depicted in Fig. 12.

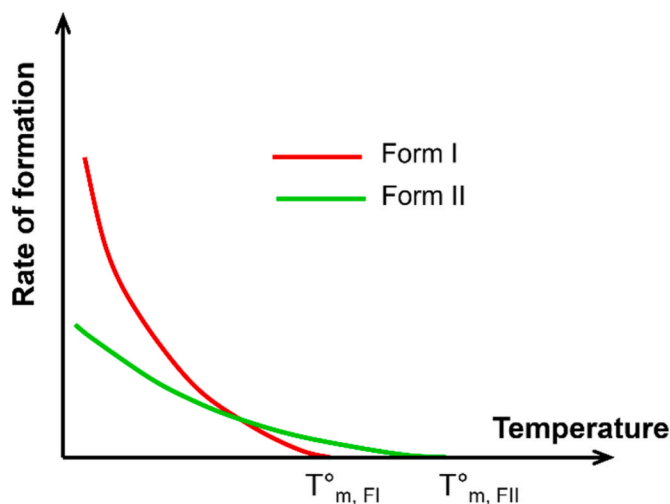


Fig. 12. Schematic change of the formation rates as a function of temperature for the two polymorphs (Form I, Form II) of a TPU with a given HS content (higher than 50 wt%). The equilibrium melting temperatures of the two structures are also indicated.

5. Conclusions

In this work, we have investigated the role of hard segment content and cooling rate on the polymorphism of TPUs based on MDI/BD, constructing a “structural map” in the cooling rate/HS content space. The quenched amorphous materials display one glass transition temperature in the entire composition range with 30–80 % HS content, showing a linear relationship between T_g and HS content. These results might indicate that the HS and SS are miscible in the melt and when they are rapidly quenched into the amorphous state.

All the materials can crystallize, displaying one or two crystallization peaks depending on the previous cooling rate and HS content. They show a complex melting behavior with several peaks arising from the two crystalline forms and reorganization processes during the scan. Employing cooling rates below approximately 10 K/min, Forms I and II are obtained, as confirmed by WAXD. As proven by PLOM, Form II exhibits a spherulitic superstructure, while Form I is non-birefringent.

The kinetics of the two polymorphs allow the suppression of the formation of Form II by increasing the cooling rate to 10–1000 K/min. Eventually, ordering can be entirely suppressed by employing even higher cooling rates. Generally, this study provides guidelines for designing TPU materials with tailored properties thanks to the gained detailed knowledge of their non-isothermal polymorphic solidification.

CRedit authorship contribution statement

Zakarya Baouch: Writing – review & editing, Writing – original draft, Methodology, Investigation. **Katalee Jariyavidyanont:** Writing – review & editing, Writing – original draft, Methodology, Investigation. **Lisa Moni:** Investigation, Formal analysis. **Leire Sangroniz:** Writing – review & editing, Investigation, Formal analysis, Data curation. **Elmar Pösel:** Writing – review & editing, Resources, Funding acquisition. **Alejandro Müller:** Writing – review & editing, Resources, Conceptualization. **René Androsch:** Writing – review & editing, Formal analysis, Data curation, Conceptualization. **Dario Cavallo:** Writing – review & editing, Writing – original draft, Supervision, Resources, Formal analysis, Data curation, Conceptualization.

Declaration of competing interest

We declare no competing financial interest.

Acknowledgements

The work was partly funded by the Deutsche Forschungsgemeinschaft (DFG, German Research Foundation) – 439920697; 464908856. We acknowledge the European Synchrotron Radiation Facility (ESRF) for provision of synchrotron radiation facilities under proposal number MA-6191 and we would like to thank Dr. Martin Rosenthal for assistance and support in using beamline BM-26.

The University of Genova is kindly acknowledged for the contribution to the acquisition of an NMR instrument (D.R. 3404 July 19, 2018). We thank Mr. Andrea Galatini for his collaboration with NMR spectra.

Appendix A. Supplementary data

Supplementary data to this article can be found online at <https://doi.org/10.1016/j.polymer.2025.128477>.

Data availability

Data will be made available on request.

References

- [1] Z.S. Petrović, J. Ferguson, Polyurethane elastomers, *Prog. Polym. Sci.* 16 (5) (1991) 695–836, [https://doi.org/10.1016/0079-6700\(91\)90011-9](https://doi.org/10.1016/0079-6700(91)90011-9).
- [2] I. Yilgör, E. Yilgör, G.L. Wilkes, Critical parameters in designing segmented polyurethanes and their effect on morphology and properties: a comprehensive review, *Polymer* 58 (2015) A1–A36, <https://doi.org/10.1016/j.polymer.2014.12.014>.
- [3] D.S. Huh, S.L. Cooper, Dynamic mechanical properties of polyurethane block polymers, *Polym. Eng. Sci.* 11 (5) (1971) 369–376, <https://doi.org/10.1002/pen.760110504>.
- [4] R. Bonart, E.H. Müller, Phase separation in urethane elastomers as judged by low-angle X-Ray scattering. II. Experimental results, *J. Macromol. Sci. Part B* 10 (2) (1974) 345–357, <https://doi.org/10.1080/00222347408260835>.
- [5] Y. Camberlin, J.P. Pascault, Quantitative DSC evaluation of phase segregation rate in linear segmented polyurethanes and polyurethaneureas, *J. Polym. Sci. Polym. Chem. Ed.* 21 (2) (1983) 415–423, <https://doi.org/10.1002/pol.1983.170210211>.
- [6] L.M. Leung, J.T. Koberstein, Small-angle scattering analysis of hard-microdomain structure and microphase mixing in polyurethane elastomers, *J. Polym. Sci. Polym. Phys. Ed* 23 (9) (1985) 1883–1913, <https://doi.org/10.1002/pol.1985.180230912>.
- [7] L.M. Leung, J.T. Koberstein, DSC annealing study of microphase separation and multiple endothermic behavior in polyether-based polyurethane block copolymers, *Macromolecules* 19 (3) (1986) 706–713, <https://doi.org/10.1021/ma00157a038>.
- [8] T. Takahashi, N. Hayashi, S. Hayashi, Structure and properties of shape-memory polyurethane block copolymers, *J. Appl. Polym. Sci.* 60 (7) (1996) 1061–1069, [https://doi.org/10.1002/\(SICI\)1097-4628\(19960516\)60:7<1061::AID-APP18>3.0.CO;2-3](https://doi.org/10.1002/(SICI)1097-4628(19960516)60:7<1061::AID-APP18>3.0.CO;2-3).
- [9] J.W. Cho, J.W. Kim, Y.C. Jung, N.S. Goo, Electroactive shape-memory polyurethane composites incorporating carbon nanotubes, *Macromol. Rapid Commun.* 26 (5) (2005) 412–416, <https://doi.org/10.1002/marc.200400492>.
- [10] J. Blackwell, M.R. Nagarajan, T.B. Hoitink, Structure of polyurethane elastomers: effect of chain extender length on the structure of MDI/diol hard segments, *Polymer* 23 (7) (1982) 950–956, [https://doi.org/10.1016/0032-3861\(82\)90392-5](https://doi.org/10.1016/0032-3861(82)90392-5).
- [11] R.M. Briber, E.L. Thomas, Investigation of two crystal forms in MDI/BDO-based polyurethanes, *J. Macromol. Sci. Part B* 22 (4) (1983) 509–528, <https://doi.org/10.1080/00222348308224773>.
- [12] J. Blackwell, C.D. Lee, Hard-segment polymorphism in MDI/Diol-Based polyurethane elastomers, *J. Polym. Sci. Polym. Phys. Ed* 22 (4) (1984) 759–772, <https://doi.org/10.1002/pol.1984.180220417>.
- [13] R.M. Briber, E.L. Thomas, The structure of MDI/BDO-based polyurethanes: diffraction studies on model compounds and oriented thin films, *J. Polym. Sci. Polym. Phys. Ed* 23 (9) (1985) 1915–1932, <https://doi.org/10.1002/pol.1985.180230913>.
- [14] M.W. Terban, R. Dabbous, A.D. Debellis, E. Pösel, S.J.L. Billinge, Structures of hard phases in thermoplastic polyurethanes, *Macromolecules* 49 (19) (2016) 7350–7358, <https://doi.org/10.1021/acs.macromol.6b00889>.
- [15] Z. Wang, X. Li, E. Pösel, B. Eling, T. Liao, Z. Wang, Polymorphic microstructure of MDI/BD-Block polyurethane as determined by temperature-sensitive conformation variation, *Soft Matter* 17 (41) (2021) 9447–9456, <https://doi.org/10.1039/D1SM01283E>.
- [16] J.T. Koberstein, A.F. Galambos, Multiple melting in segmented polyurethane block copolymers, *Macromolecules* 25 (21) (1992) 5618–5624, <https://doi.org/10.1021/ma00047a010>.
- [17] A. Saiani, W.A. Daunch, H. Verbeke, J.-W. Leenslag, J.S. Higgins, Origin of multiple melting endotherms in a high hard block content polyurethane. 1. Thermodynamic investigation, *Macromolecules* 34 (26) (2001) 9059–9068, <https://doi.org/10.1021/ma0105993>.
- [18] A. Saiani, C. Rochas, G. Eeckhaut, W.A. Daunch, J.-W. Leenslag, J.S. Higgins, Origin of multiple melting endotherms in a high hard block content polyurethane. 2. Structural investigation, *Macromolecules* 37 (4) (2004) 1411–1421, <https://doi.org/10.1021/ma034604+>.
- [19] Y. Swolfs, E. Bertels, I. Verpoest, B. Goderis, Linking the morphology of a high hard segment content polyurethane to its thermal behaviour and mechanical properties, *Polymer* 81 (2015) 1–11, <https://doi.org/10.1016/j.polymer.2015.11.007>.
- [20] J. Balko, B. Fernández-d’Arlas, E. Pösel, R. Dabbous, A.J. Müller, T. Thurn-Albrecht, Clarifying the origin of multiple melting of segmented thermoplastic polyurethanes by fast scanning calorimetry, *Macromolecules* 50 (19) (2017) 7672–7680, <https://doi.org/10.1021/acs.macromol.7b00871>.
- [21] F. Liu, X. Liao, Q. Peng, Y. Zhao, S. Li, G. Li, Effect of two crystalline forms on the multiple melting and crystallization kinetics of thermoplastic polyurethane, *Cryst. Growth Des.* 22 (10) (2022) 6015–6022, <https://doi.org/10.1021/acs.cgd.2c00654>.
- [22] Z. Wang, X. Li, E. Pösel, B. Eling, Z. Wang, Melting behavior of polymorphic MDI/BD-Block TPU investigated by using in-Situ SAXS/WAXS and FTIR techniques. Hydrogen bonding formation causing the inhomogeneous melt, *Polym. Test.* 96 (2021) 107065, <https://doi.org/10.1016/j.polymertesting.2021.107065>.
- [23] F. Liu, S. Li, X. Liao, Q. Peng, G. Li, Investigation on the crystallization behavior and detail spherulitic morphology of two crystal forms of thermoplastic polyurethanes, *J. Polym. Res.* 29 (7) (2022) 262, <https://doi.org/10.1007/s10965-022-03112-4>.
- [24] J. Foks, H. Janik, R. Morphology Russo, Thermal and mechanical properties of solution-cast polyurethane films, *Eur. Polym. J.* 26 (3) (1990) 309–314, [https://doi.org/10.1016/0014-3057\(90\)90246-Z](https://doi.org/10.1016/0014-3057(90)90246-Z).
- [25] B. Chen, J. Jiang, Z. Wang, Y. Li, F. Tian, L. Wang, W. Zhai, Controlling the crystal morphology of high-hardness TPU through two pre-crystallization processes and its

- impact on physical foaming behavior, *Polymer* 305 (2024) 127172, <https://doi.org/10.1016/j.polymer.2024.127172>.
- [26] A. Begenir, S. Michiels, B. Pourdeyghi, Crystallization behavior of elastomeric block copolymers: thermoplastic polyurethane and polyether-block-amide, *J. Appl. Polym. Sci.* 111 (3) (2009) 1246–1256, <https://doi.org/10.1002/app.29082>.
- [27] M.A. Hood, B. Wang, J.M. Sands, J.J.L. Scala, F.L. Beyer, C.Y. Li, Morphology control of segmented polyurethanes by crystallization of hard and soft segments, *Polymer* 51 (10) (2010) 2191–2198, <https://doi.org/10.1016/j.polymer.2010.03.027>.
- [28] B. Fernández-d'Arlas, R.P. Baumann, E. Pösel, A.J. Müller, Influence of composition on the isothermal crystallisation of segmented thermoplastic polyurethanes, *CrystEngComm* 19 (32) (2017) 4720–4733, <https://doi.org/10.1039/C7CE01028A>.
- [29] A. Stribeck, B. Eling, E. Pösel, M. Malfois, E. Schander, Melting, solidification, and crystallization of a thermoplastic polyurethane as a function of hard segment content, *Macromol. Chem. Phys.* 220 (11) (2019) 1900074, <https://doi.org/10.1002/macp.201900074>.
- [30] W.P. Yang, C.W. Macosko, S.T. Wellinghoff, Thermal degradation of urethanes based on 4,4'-Diphenylmethane diisocyanate and 1,4-Butanediol (MDI/BDO), *Polymer* 27 (8) (1986) 1235–1240, [https://doi.org/10.1016/0032-3861\(86\)90012-1](https://doi.org/10.1016/0032-3861(86)90012-1).
- [31] Y. Camberlin, J.P. Pascault, J.M. Letoffe, P. Claudy, Synthesis and DSC study of model hard segments from diphenyl methane diisocyanate and butane diol, *J. Polym. Sci. Polym. Chem. Ed.* 20 (2) (1982) 383–392, <https://doi.org/10.1002/pol.1982.170200212>.
- [32] K.K.S. Hwang, G. Wu, S.B. Lin, S.L. Cooper, Synthesis and characterization of MDI-butenediol urethane model compounds, *J. Polym. Sci. Polym. Chem. Ed.* 22 (7) (1984) 1677–1697, <https://doi.org/10.1002/pol.1984.170220714>.
- [33] G. Portale, D. Cavallo, G.C. Alfonso, D. Hermida-Merino, M. van Drongelen, L. Balzano, G.W.M. Peters, J.G.P. Goossens, W. Bras, Polymer crystallization studies under processing-relevant conditions at the SAXS/WAXS DUBBLE beamline at the ESRF, *J. Appl. Crystallogr.* 46 (6) (2013) 1681–1689, <https://doi.org/10.1107/S0021889813027076>.
- [34] C. Li, J. Han, Q. Huang, H. Xu, J. Tao, X. Li, Microstructure development of thermoplastic polyurethanes under compression: the influence from first-order structure to aggregation structure and a structural optimization, *Polymer* 53 (5) (2012) 1138–1147, <https://doi.org/10.1016/j.polymer.2012.01.019>.
- [35] A.M. de Ilarduya, E. Carvalho, A. Alla, S. Muñoz-Guerra, Sequence analysis of polyether-based thermoplastic polyurethane elastomers by ¹³C NMR, *Macromolecules* 43 (8) (2010) 3990–3993, <https://doi.org/10.1021/ma100395x>.
- [36] T.K. Chen, J.Y. Chui, T.S. Shieh, Glass transition behaviors of a polyurethane hard segment based on 4,4'-Diisocyanatodiphenylmethane and 1,4-Butanediol and the calculation of microdomain composition, *Macromolecules* 30 (17) (1997) 5068–5074, <https://doi.org/10.1021/ma9618639>.
- [37] B. Fernández-d'Arlas, J. Maiz, R.A. Pérez-Camargo, R.-P. Baumann, E. Pösel, R. Dabbous, A. Stribeck, A.J. Müller, SSA fractionation of thermoplastic polyurethanes, *Polym. Cryst.* 4 (1) (2021) e10148, <https://doi.org/10.1002/pcr2.10148>.
- [38] H. Wang, L. Zhang, K.W.E. Peh, Q. Yu, Y. Lu, W. Hua, Y. Men, Effect of phase separation and crystallization on enthalpy relaxation in thermoplastic polyurethane, *Macromolecules* 55 (19) (2022) 8566–8576, <https://doi.org/10.1021/acs.macromol.2c01504>.
- [39] K.N. Raftopoulos, B. Janowski, L. Apekis, K. Pielichowski, P. Pissis, Molecular mobility and crystallinity in polytetramethylene ether glycol in the bulk and as soft component in polyurethanes, *Eur. Polym. J.* 47 (11) (2011) 2120–2133, <https://doi.org/10.1016/j.eurpolymj.2011.07.020>.
- [40] W. MacKnight, M. Yang, T. Kajiyama, *Amer. Chem. Soc. Polym. Prepr.* 9 (1968) 860.
- [41] J.E.K. Schawe, S. Ziegelmeier, Determination of the thermal short time stability of polymers by fast scanning calorimetry, *Thermochim. Acta* 623 (2016) 80–85, <https://doi.org/10.1016/j.tca.2015.11.020>.